


Article

Effect of Cooling Rate and Modification by Strontium on the Thermal Conductivity of Al-8Si Alloy

Guanyi Wang^{1,2}, Zhiping Guan^{1,2} , Jinguo Wang^{1,2}, Mingwen Ren², Ruifang Yan² and Jiawang Song^{1,*}

¹ State Key Laboratory of Automotive Simulation and Control, Jilin University, Changchun 130022, China; wgy1vc@126.com (G.W.); guanzp@jlu.edu.cn (Z.G.); jgwang@jlu.edu.cn (J.W.)

² School of Materials Science and Engineering, Jilin University, Changchun 130022, China; renmw@jlu.edu.cn (M.R.); yanruifang@jlu.edu.cn (R.Y.)

* Correspondence: songjw@jlu.edu.cn

Abstract: Cooling rate plays a critical role in determining the thermal conductivity of Al-Si alloys. Although the effect of morphology and size of Si (changed by heat treatment) on its thermal conductivity has been investigated, the effect of cooling rates on thermal conductivity has not been well studied. In this study, we investigated the microstructure of an Al-8Si (with and without modification by Strontium (Sr)) alloy with cooling rates from 46.2 °C/s to 234 °C/s. It was found that the effect of cooling rate on thermal conductivity of Sr modification and Sr-free samples are opposite from each other. As a result, while the cooling rate increased from 46.2 °C/s to 234 °C/s, the calculated thermal conductivity increased from 145.3 MS/m to 151.5 MS/m for Sr-free Al-8Si alloy, and the calculated thermal conductivity was reduced from 187.5 MS/m to 176.7 MS/m for the Sr-modified Al-8Si alloy. By discussing how thermal conductivity correlates with eutectic silicon morphology and secondary dendrite arm spacing, the relationship between cooling rate and thermal conductivity were explained. This work suggests a new design strategy for improving the thermal conductivity of Al-Si hypoeutectic alloys.



Citation: Wang, G.; Guan, Z.; Wang, J.; Ren, M.; Yan, R.; Song, J. Effect of Cooling Rate and Modification by Strontium on the Thermal Conductivity of Al-8Si Alloy. *Metals* **2021**, *11*, 1334. <https://doi.org/10.3390/met11091334>

Academic Editor: Andrey Belyakov

Received: 29 July 2021

Accepted: 20 August 2021

Published: 24 August 2021

Publisher's Note: MDPI stays neutral with regard to jurisdictional claims in published maps and institutional affiliations.



Copyright: © 2021 by the authors. Licensee MDPI, Basel, Switzerland. This article is an open access article distributed under the terms and conditions of the Creative Commons Attribution (CC BY) license (<https://creativecommons.org/licenses/by/4.0/>).

Keywords: Al-Si alloy; cooling rate; modification; thermal conductivity; microstructure

1. Introduction

Al-Si alloys usually present good thermal/electrical conductivity as well as excellent casting properties [1–4]. As a structural material, it has light-weight structural materials with low cost. Additionally, Al-Si alloys have a wide range of applications in industries such as automobiles, construction, and communications [5]. Especially since 5G base stations in communication began springing up all over the world recently, aluminum alloy-based radiators are required to possess excellent thermal conductivity due to high power consumption and severe heat generation [6–8], along with enough mechanical properties and a light weight. Al-Si hypoeutectic alloys are a potential and powerful candidate for the requirement of radiators in 5G base stations. Therefore, it is important to determine how to improve the thermal conductivity of Al-Si hypoeutectic alloys.

Generally, thermal conductivity is mainly controlled by the mobility of electrons, lattice elastic vibration (phonons), and heat dissipation process. Since the contribution of phonons is negligible for metals or alloys, the thermal conductivity is mainly affected by the mobility of electrons. For Al alloys, the mobility of electrons usually depends on the solid solution degree of solute elements in Al matrix, which has been investigated thoroughly in the past few decades [9,10]. However, when the chemical composition of solute elements is fixed for a given Al-Si hypoeutectic alloy, it is generally believed that the micro-structures of the alloy play a decisive role on the thermal conductivity, for example the morphology and size of the Si phase [7,11,12], and the density of defects such as grain boundary and phase boundary [10,13], which can be reflect by the secondary dendrite arm spacing (SDAS) in as-cast conditions.

The control of microstructures of Al-Si hypoeutectic alloys is mainly implemented through a casting process or heating treatment. It can be refined and spheroidized by solid solution or/and aging treatment, and different heat treatment processes result in Si particles with different sphericities, which also has significant impact on the thermal conductivity of the alloy [12,14,15]. In addition, Vandersluis et al. [16] studied the effect of cooling rate of solidification on thermal conductivity by controlling the mold temperature, which revealed that the Si particles are longer and larger at higher mold temperatures. After the heat treatment, the long needle shaped eutectic silicon particles are broken down into smaller ones and then gradually spheroidized, which improves the thermal conductivity of the alloy.

The morphology of the eutectic silicon in Al-Si alloys can also be influenced by modification, leading to significant changes in the thermal conductivity. Guo et al. [7] found that the eutectic Si changes from a long needle shape to a short rod shape due to the addition of Sr, which reduces the scattering effect of electrons and improves the thermal conductivity of the alloy. Wang et al. [14] found that the addition of Sr can effectively increase the thermal conductivity of Al-Si hypoeutectic alloys, due to the formation of $\text{Al}_2\text{Si}_2\text{Sr}$ phases on the surface of silicon. They inferred that the addition of Sr increases the contribution of free electron migration to the thermal conductivity. Additionally, the SDAS, which is controlled by cooling rate or modification, also has a great influence on the thermal conductivity of Al-Si alloys. Some researchers studied the changes in the thermal conductivity of alloys with cooling rates during solidification in the range of (0.127–8.25 K/s) [17]. However, they did not find a significant effect of the increase in the cooling rates during solidification on the thermal conductivity, which means that although the rise of the cooling rate increases the number of paths for thermal energy carriers (electrons), the decrease in SDAS might offset this increase.

For Al-Si hypoeutectic alloys, as mentioned above, the morphology and the size of eutectic silicon as well as the SDAS which matter to the thermal conductivity are significantly influenced by both cooling rates during solidification and modification by Sr elements. However, it is not clear which degree of influence is more significant if comparing cooling rate with modification by Sr element. Moreover, cooling rates may also cause different modification mechanisms [18,19], which indicates that the influences of cooling rates and modification on the thermal conductivity are coupling and complicated. In this study, therefore, the individual/coupling influences of cooling rates and modification by Sr element on the thermal conductivity of Al-Si hypoeutectic alloys will be investigated, which aims to clarify the mechanism for linking microstructures with the thermal conductivity, and evaluate the degree of their individual/coupling influences. In the investigation, the as-cast Al-8Si hypoeutectic alloy is chosen, without addition of any other alloy elements and without heating treatment. It is guaranteed that only the two factors of cooling rates and modification by Sr element will be investigated, excluding the influences of other factors on the thermal conductivity.

2. Materials and Methods

In this paper, a resistance furnace (SG2-7-12, Rongfeng, Shanghai, China) was used to melt the alloy. Pure Al (99.8%) and Al-24.4Si master alloys were used to prepare the Al-8Si alloy (wt.% unless otherwise specified, used throughout the paper). Firstly, pure Al and Al-24.4Si master alloys were put into a graphite crucible and heated to 800 °C in a resistance furnace. As the alloy started melting, the temperature was adjusted to 750 °C. After the alloy was completely melted, Al-10Sr alloy wrapped in aluminum foil was added (this step was omitted when there was no Sr modification). The alloy was stirred well and kept at temperature for 15 min. Finally, high-purity Ar was passed into the melt to degas for 2 min. After the slag was removed, the melt was poured into a variable thickness water-cooled copper mold with a length of 50 mm and a height of 80 mm (there is a hole at the bottom of the mold for inserting a thermocouple). K-type thermocouple and a data acquisition hardware (EM9104C, ZTIC, Beijing, China) were used to set the data acquisition frequency

to 50 Hz to measure the real-time temperatures of cooling during solidification. Four Al-8Si alloys and Al-8Si-0.08Sr alloys with different thicknesses of 5 mm, 10 mm, 15 mm, and 20 mm were obtained. During the above operation, two brand new crucibles were used to avoid the introduction of impurities, and all of the tools that were in contact with the melt were coated with ZnO on the surface and heated and dried in advance. After the sample preparation was completed, a spectrum analyzer (ARL 4460, Ecublens, Ecublens, Switzerland) was used to determine the composition of the sample. At least 4 points was measured of each sample, and the average value was calculated. The measurement results are shown in Table 1. Samples for SEM observation were prepared by traditional grinding and polishing. The polished sample was deeply corroded in 5 vol.% HF aqueous solution.

Table 1. Chemical compositions of Al-8Si alloys (wt.%).

Alloy	Si	Fe	Cu	Mg	Mn	Ti	Sr	Al
Al-8Si	7.97	0.21	0.004	0.001	0.004	0.001	-	Bal.
Al-8Si-0.08Sr	8.08	0.18	0.004	0.001	0.003	0.001	0.081	Bal.

The microstructure of eutectic Si was observed by scanning electron microscope (SEM, Zeiss Evo 18, Zeiss, Jena, Germany), and the average diameter and shape factor were measured by image-pro plus software (6.0, Media Cybernetics, Rockville, MD, USA). The shape factor (S) is defined as follows

$$S = 4\pi A/P^2 \quad (1)$$

where S , A and P are the shape factor, area and perimeter of a single eutectic silicon phase. More than 5 photos and 500 particles were measured in each sample.

The samples were re-ground and re-polished by traditional grinding and polishing, and the as-polished samples were anodized in fluoroboric acid solution. It was observed by an optical microscope (OM, Carl ZEISS-Axio Imager. A2m, Jena, Germany), and its SDAS was measured by Nano Measurer 1.2 software (1.2.5, Fudan University, Shanghai, China) using the linear intercept method. The conductivity of the alloy was measured by a conductivity measuring instrument (Sigmatest 2.069, Foerster, Reutlingen, Germany) at room temperature (approximately 25 °C, and the measuring frequency is 120 Hz). More than 5 data were measured and averaged in each sample. The measurement results were converted to International Annealed Copper Standard (% IACS) and the average value was calculated. The thermal conductivity of the alloy was obtained from the electrical conductivity by the Wiedemann-Franz law.

$$\lambda = LT\sigma \quad (2)$$

where λ is the thermal conductivity, L Lorentz number, T is the temperature, and σ is the electrical conductivity. For aluminum alloy, L is $2.1 \times 10^{-8} \text{ W}\Omega\text{K}^{-2}$. In the Si-containing aluminum alloy, L increases with the increase of Si content, and L is $2.1 \times 10^{-8} + 0.021 \times 10^{-8} \times \text{wt.\% Si W}\Omega\text{K}^{-2}$. For aluminum alloys, the revised Widman-Franz law is applied [20–22].

$$\lambda = LT\sigma + c \quad (3)$$

where c is 12.6 W/(m·K). For hypoeutectic alloys, under the measurement conditions from, according to the modified Wiedemann-Franz law, there is a linear correlation between the calculated thermal conductivity and the measured value. The calculated thermal conductivity in the article was calculated by the revised Wiedemann-Franz law.

3. Results and Discussion

3.1. Cooling Rate

Figure 1 (reference colorful version) shows the cooling curves when the sample thickness is 5 mm, 10 mm, 15 mm, and 20 mm, respectively, which was measured by

the K-type thermocouple. The section above 610 °C was used to calculate the average cooling rates during solidification (610 °C is the liquidus temperature of the alloy under this composition simulated by JMatPro7.0 (Sente Software, Surrey, UK) The measurement results of the average cooling rate of the solidification of four thicknesses were about 234 °C/s, 136 °C/s, 63.2 °C/s, 46.2 °C/s. Since the temperature of the cooling water and the pouring temperature of the copper mold were fixed, the cooling rates during solidification decreases with the increase of the thickness of the sample.

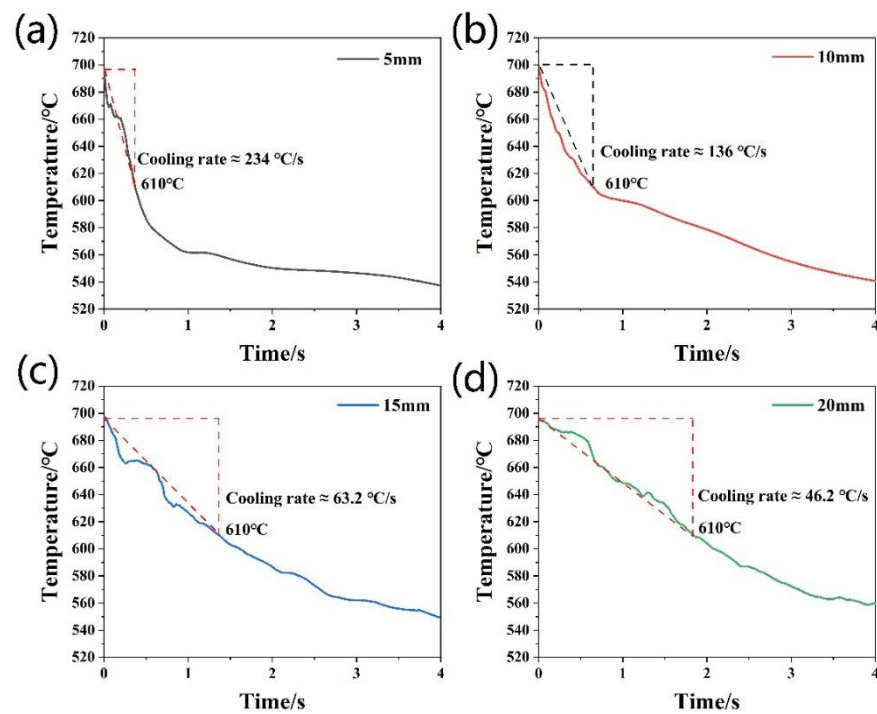


Figure 1. Cooling curves and the measurement approach of cooling rates during solidification of four different thickness of samples: (a) 5 mm, (b) 10 mm, (c) 15 mm, and (d) 20 mm.

3.2. Microstructure Characteristics

In previous studies on SDAS(λ) [23], the function of estimating the distance between secondary dendrites was summarized as follow:

$$\lambda = C_1(GV)^{-a}, \quad (4)$$

where G is thermal gradient, C_1 is constant and V is cooling rates during solidification.

Or

$$\lambda = K(t_{SL})^a, \quad (5)$$

where t_{SL} is solidification time, and K is constant. The exponent a has been recently summarized in the literature for a number of alloys [24]. It can be seen from the formula that the higher the cooling rates during solidification (the shorter the solidification time) is, in other words, the greater the degree of subcooling is, the smaller the SDAS will be. The OM photographs of the modified and unmodified samples with different cooling rates are shown in the Figure 2. Figure 2a–f can clearly show that as the cooling rate increases, the size of α -Al gradually decreases. The SDAS changes of α -Al with and without modification are showed in Figure 2. The SDAS decreases with the increase of the cooling rate. In addition, because of the addition of Sr, the SDAS of the sample with Sr added is smaller than that of the sample without Sr under the same cooling conditions. As shown in Figure 3d, when the cooling rate is 46.2 °C/s, the average SDAS of samples without Sr is 53.7 μm , while the average SDAS of samples with Sr modification is only 47.8 μm . The error bar in this paper is calculated from the standard deviation (S.D.). Similar

phenomena have also been observed in the experiments of others [25]. In the process of dendrite growth, since the addition of Sr reduces, the interfacial energy at the front of the α -Al dendrite solidification interface, the supercooling of the dendrite tip is reduced, which suppresses the nucleation of liquid equiaxed crystals and promotes the formation of columnar dendrites. During the dendrite growth process, the SDAS of columnar dendrites decreases as the increase of Sr for the same reason [7,26].

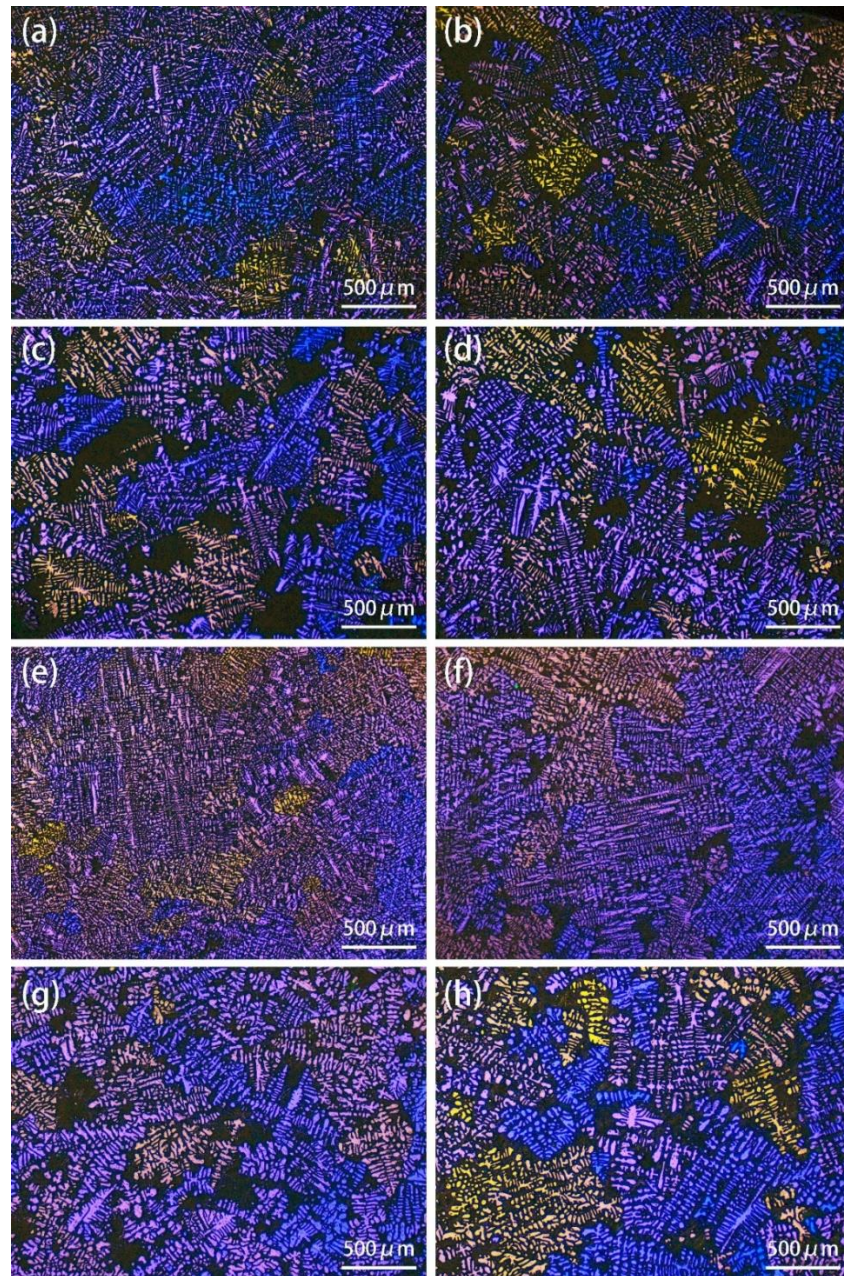


Figure 2. OM microstructure of α -Al in Al-8Si alloys under different cooling rates: (a) Sr + 234 °C/s, (b) Sr + 136 °C/s, (c) Sr + 63.2 °C/s, (d) Sr + 46.2 °C/s, (e) 234 °C/s, (f) 136 °C/s, (g) 63.2 °C/s, (h) 46.2 °C/s.

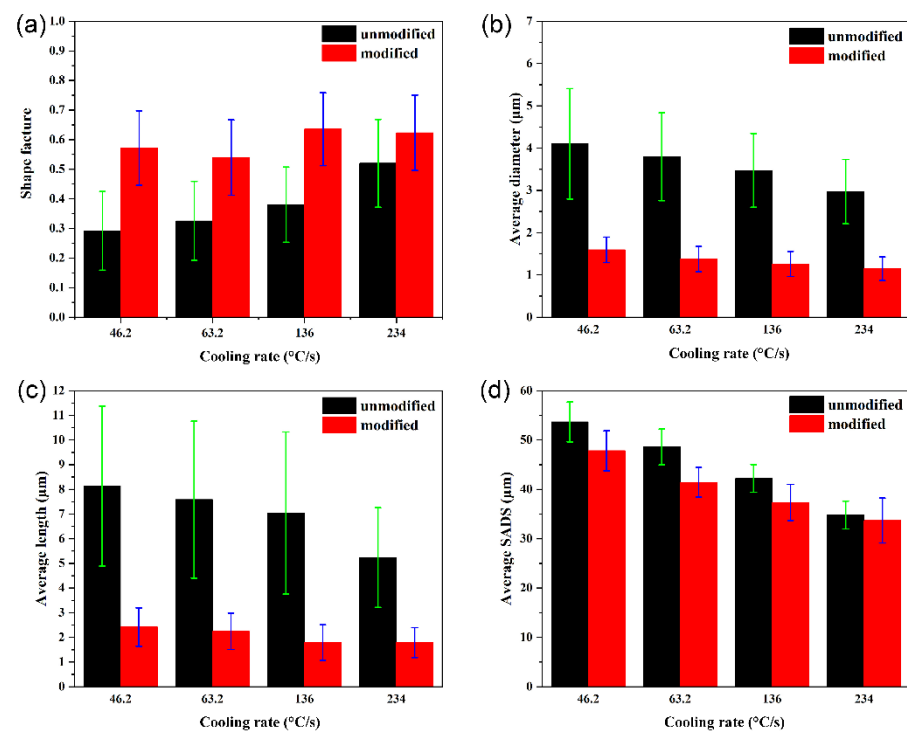


Figure 3. Eutectic silicon particles (a–c) and α -Al (d) (with and without Sr) under different cooling rates: (a) average shape factor, (b) average diameter, (c) average length, (d) average SDAS.

Figure 4 shows the SEM photographs of the alloys with different cooling rates with and without modification. Figure 4i–l shows that in the case of the unmodified alloy, as the cooling rate increases, the shape of the Si particles gradually becomes shorter, and the shape factor S also increases with the cooling rate (Figure 3a). It can be seen from Figure 4a–h that eutectic silicon is mainly formed by fibrous shape, short rod shape and nearly spherical shape with the addition of Sr, and the shape factor S is not significantly related to the change of the cooling rate. As is showed in Figure 3b, the Si particle size decreases slightly with the increase of cooling rate. As the cooling rate increased from 46.2 °C/s to 234 °C/s, the average diameter of Si in the unmodified samples decreased from 4.1 μm to 2.9 μm , while the average diameter of the Sr modified samples only decreased from 1.6 μm to 1.2 μm . The changes of particle length are shown in Figure 3c. As the cooling rate increases from 46.2 °C/s to 234 °C/s, the average length of Si in the unmodified sample decreases from 8.1 μm to 5.2 μm , while the average length of the Sr-containing sample only decreases from 2.41 μm to 1.79 μm . In the unmodified sample, Si crystals are grown in the $\langle 112 \rangle$ phase due to its facet properties. Reentrant twins can appear on the (111) crystal plane, which facilitates the formation of two-dimensional growth steps. It also facilitates the landing of Si atoms, which is twin plane re-entrant edge (TPRE) mechanism. At this time, as the cooling rate increases and the supercooling degree increases, the heterogeneous nucleation of Si becomes easier. When a large amount of Si grows up together, the Si particles have not grown for a long time before the eutectic reaction is almost over. Therefore, the length of Si is significantly reduced when the cooling rate is increased. Due to the TPRE mechanism of Si, the width change of Si is far less significant than the length change, and S is also significantly increased with the increase of the cooling rate [7]. In Al-Si with Sr modified, the growth mechanism of Si phase is different between the early and late growth stages. In the early growth stage, Sr adsorbs on the growth steps of Si to prevent Si from growing in steps, which reducing the effectiveness of twin planes. At this time, the shape of Si is flaky, and its growth is mainly based on the impurity-induced twinning (IIT) mechanism. The adsorption of Sr also produces a large number of twins in Si, and at this time Si turns to be dominated by the TPRE mechanism. The presence of Sr interrupts the step growth trend of

Si and has made Si sufficiently refined. At this time, the degree of subcooling on the size and morphology of Si is no longer the major factor that effect. Therefore, in the case of Sr modification, increasing the cooling rate only has a small change in length, and the shape factor does not show a significant relationship with the cooling rate.

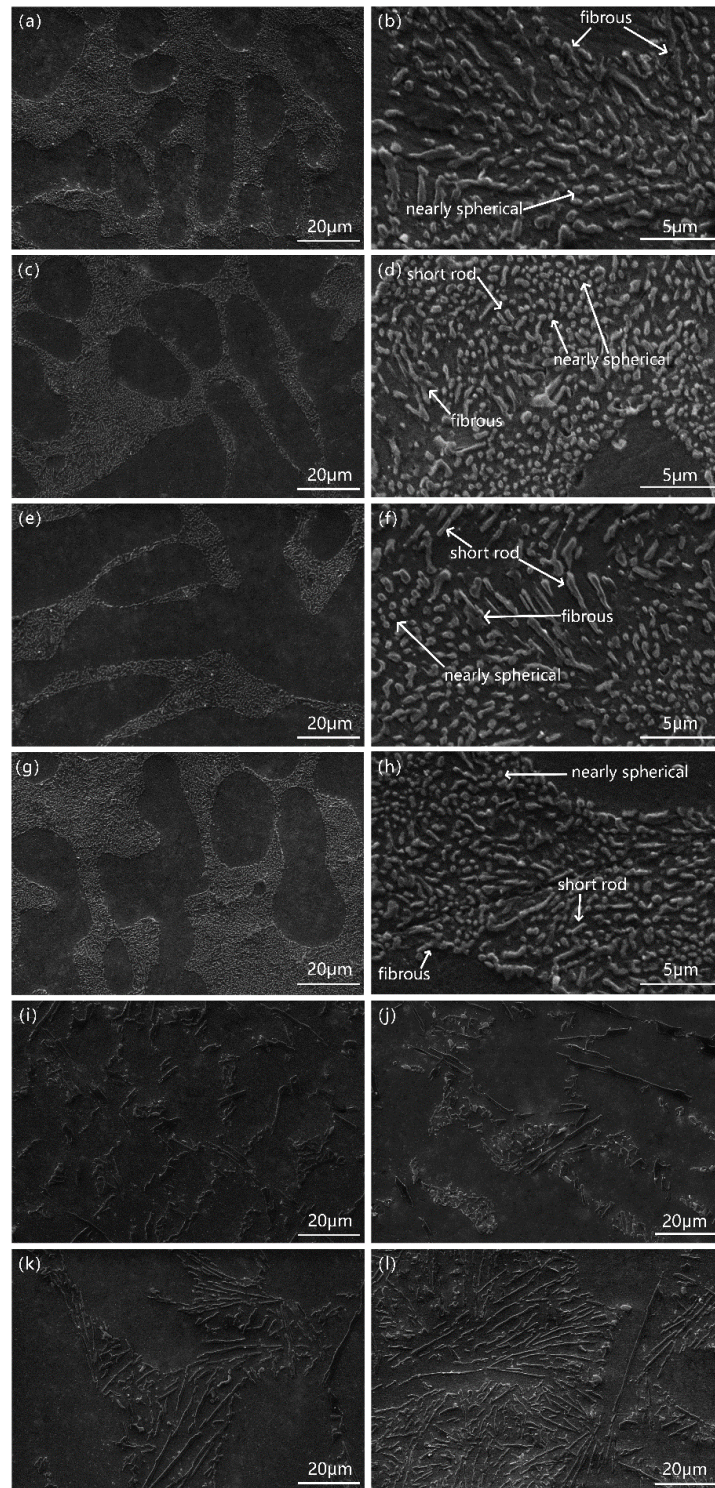


Figure 4. SEM microstructure of eutectic silicon in Al-8Si alloys under different cooling rates: (a) Sr + 234 °C/s, (b) amplification of Sr + 234 °C/s (c) Sr + 136 °C/s, (d) amplification of Sr + 136 °C/s, (e) Sr + 63.2 °C/s, (f) amplification of Sr + 63.2 °C/s, (g) Sr + 46.2 °C/s, (h) amplification of Sr + 46.2 °C/s, (i) 234 °C/s, (j) 136 °C/s, (k) 63.2 °C/s, (l) 46.2 °C/s.

3.3. Thermal and Electrical Conductivity

During the process of metal conduction and heat conduction, the main carriers of both are free electrons. When the free electron meets the vibrating atom during its motion, it will be scattered by the vibrating atom. Free electrons are affected by defects and phonon scattering to produce electronic thermal resistance. The main factor that determines its electrical conductivity and thermal conductivity is the mean free path of free electrons [27]. Any existence that destroys the integrity of the lattice structure in the alloy will increase the scattering effect of free electrons, such as point defects, solid solution atoms, grain boundaries, phase boundaries and so on. Figure 5 shows the % IACS conductivity and calculated thermal conductivity of modified and unmodified samples under different cooling rates. Figure 6a,b illustrates the phenomenon that occurs when electrons meet Si particles. With the increase of cooling rates during solidification, as the Si particle size in the unmodified alloy becomes smaller and the shape factor S increases, its blocking and scattering effects on electrons become weaker. The mean free path of electrons increases, and the conductivity increases accordingly. The electrical conductivity and thermal conductivity of all modified alloys are higher than that of the unmodified alloys, as shown in Figure 5. The diameter, S and length of the Si particle of the modified alloy at all cooling rates are smaller than those of the unmodified alloy. Based on the research results of others [7,12,15], reducing the particle size or increasing the shape factor through heat treatment will cause the increase of electrical conductivity, which is also accord with the research results in unmodified alloys.

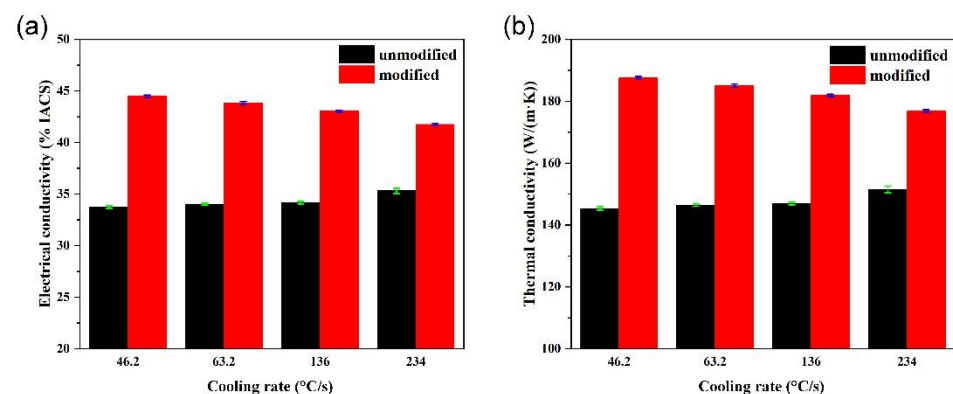


Figure 5. Properties of samples (with and without Sr) under different cooling rates: (a) electrical conductivity and (b) thermal conductivity.

It is worth noticing that in the modified alloy, the size and shape of the Si particles change with the cooling rate. However, the change is not as obvious as that in the unmodified alloy. The change trend of electrical conductivity and thermal conductivity with cooling rates during solidification of modified alloys is opposite to that of unmodified alloys (as shown in Figure 5). Compared with heat treatment, except for the change in the size of Si particles, under the effect of increased undercooling the increase in cooling rates during solidification promotes the heterogeneous nucleation of Si while also promotes the heterogeneous nucleation of α -Al and the decrease of both grain size and SDAS. With the increase of cooling rate, the grain size, the secondary dendrite arm spacing (SDAS) of α -Al and the size of Si particles all decreased (which, in a way, means the density of grain and phase boundaries inside the alloy is increased). The experimental results also prove that when the cooling rate increases from 46.2 °C/s to 234 °C/s, the SDAS decreases from 47.83 μm to 33.68 μm (Figure 3d). As two kinds of defect, grain boundary and phase boundary also have a scattering effect on the movement of electrons. In Figure 6c, the dendrite has a small interface density and the electrons are more likely to be scattered when passing through, which leads to a decrease in conductivity. In Figure 6d, the size of dendrites is larger and the number of interfaces is smaller, and electrons can easily pass through. The size and shape of the modified alloy Si particles are not significantly affected by the cooling rate. Due to the increase of grain boundary and phase boundary density,

the opposite phenomenon from unmodified sample is shown in the modified one that the thermal conductivity of the modified alloy decreases with the increase of cooling rate.

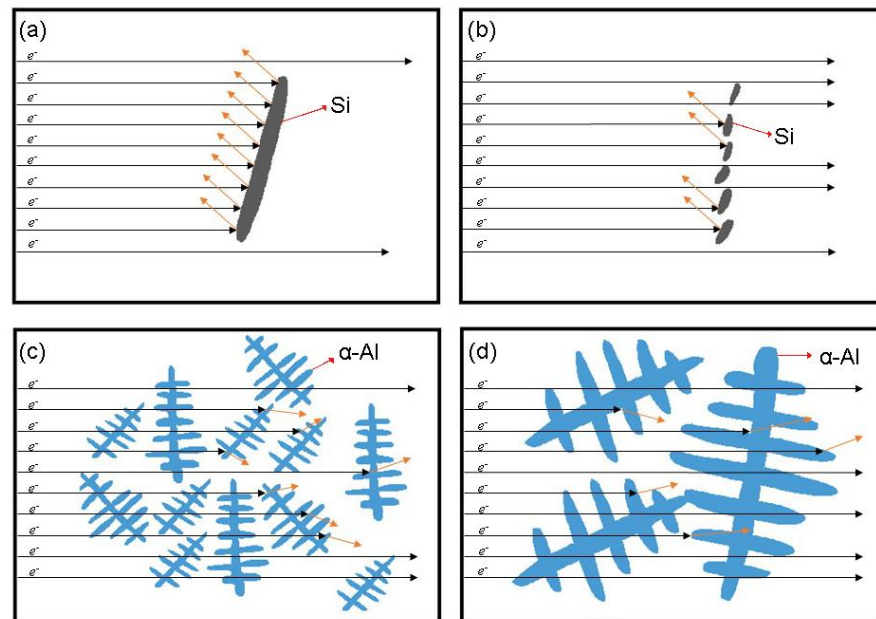


Figure 6. Schematic diagrams of electrons being scattered by: (a) eutectic silicon particles under a slower cooling rate, (b) eutectic silicon particles under a faster cooling rate, (c) α -Al grain boundary under a faster cooling rate, and (d) α -Al grain boundary under a slower cooling rate.

4. Conclusions

In this work, we studied the effects of different cooling rates and the effects of modification (with/without Sr) on the microstructure and thermal conductivity of Al-8Si alloys. For the Sr-free Al-8Si alloy, while the cooling rate increased from 46.2 °C/s to 234 °C/s, the average length of Si particles reduced from 8.1 μm to 5.2 μm , the average diameter reduced from 4.1 μm to 2.9 μm , and the shape factor S increased from 0.29 to 0.52. These changes have improved the thermal conductivity and electrical conductivity of the alloy. For the Al-8Si alloy modified by Sr, the cooling rate increased from 46.2 °C/s to 234 °C/s, the average length and average diameter of Si particles also reduced. However, the average length only reduced from 2.4 μm to 1.8 μm , and the average diameter only reduced from 1.6 μm to 1.1 μm . The shape factor S does not change significantly with the cooling rate. Due to the increase of the cooling rate, the grain refinement, the SDAS decrease, and the grain boundary phase boundary density increased, which increased the scattering effect of electrons, resulting in a decrease in thermal conductivity and electrical conductivity. Although the same situation occurs in unmodified alloys, since the increase of the cooling rates have a significant impact on the morphology and size of Si particles, the change of thermal conductivity and electrical conductivity mainly depends on the change of Si particles in this case. The research in this article can provide references for how the cooling rate affects the microstructure of Al-Si alloys and how to improve the thermal conductivity and electrical conductivity of Al-Si hypoeutectic alloys.

Author Contributions: Conceptualization, G.W. and Z.G.; methodology, G.W., J.W. and Z.G.; software, G.W. and Z.G.; validation, G.W., R.Y. and M.R.; investigation, G.W., J.S. and Z.G.; writing—original draft preparation, G.W.; writing—review and editing, G.W., J.W. and Z.G.; supervision, Z.G. and J.S.; project administration, Z.G. and J.W.; funding acquisition, Z.G. All authors have read and agreed to the published version of the manuscript.

Funding: This research was supported by the National Key Research and Development Program of China (Grant No. 2018YFB2001801).

Institutional Review Board Statement: Not applicable.

Informed Consent Statement: Not applicable.

Data Availability Statement: Not applicable.

Conflicts of Interest: The authors declare that there are no conflict of interest regarding the publication of this paper.

References

1. Cui, X.; Cui, H.; Wu, Y.; Liu, X. The improvement of electrical conductivity of hypoeutectic Al-Si alloys achieved by composite melt treatment. *J. Alloys Compd.* **2019**, *788*, 1322–1328. [[CrossRef](#)]
2. Javidani, M.; Larouche, D. Application of cast Al–Si alloys in internal combustion engine components. *Int. Mater. Rev.* **2014**, *59*, 132–158. [[CrossRef](#)]
3. Cerri, E.; Evangelista, E.; Spigarelli, S.; Cavaliere, P.; DeRiccardis, F. Effects of thermal treatments on microstructure and mechanical properties in a thixocast 319 aluminum alloy. *Mater. Sci. Eng. A* **2000**, *284*, 254–260. [[CrossRef](#)]
4. Vandersluis, E.; Lombardi, A.; Ravindran, C.; Bois-Brochu, A.; Chiesa, F.; MacKay, R. Factors influencing thermal conductivity and mechanical properties in 319 Al alloy cylinder heads. *Mater. Sci. Eng. A* **2015**, *648*, 401–411. [[CrossRef](#)]
5. Li, K.; Li, W.; Zhang, G.; Zhu, W.; Zheng, F.; Zhang, D.; Wang, M. Effects of Si phase refinement on the plasma electrolytic oxidation of eutectic Al-Si alloy. *J. Alloys Compd.* **2019**, *790*, 650–656. [[CrossRef](#)]
6. Qi, M.; Kang, Y.; Li, J.; Shang, B. Improvement in mechanical, thermal conductivity and corrosion performances of a new high-thermally conductive Al-Si-Fe alloy through a novel R-HPDC process. *J. Mater. Process. Technol.* **2020**, *279*, 116586. [[CrossRef](#)]
7. Guo, J.; Guan, Z.-P.; Yan, R.-F.; Ma, P.-K.; Wang, M.-H.; Zhao, P.; Wang, J.-G. Effect of Modification with Different Contents of Sb and Sr on the Thermal Conductivity of Hypoeutectic Al-Si Alloy. *Metals* **2020**, *10*, 1637. [[CrossRef](#)]
8. Qin, R.; Yan, R.-F.; Guan, Z.-P.; Zhang, G.-Q.; Song, J.-W.; Ren, M.-W.; Wang, J.-G. Effect of vanadium on Fe-rich phase, mechanical properties and thermal conductivity of hypoeutectic Al–Si alloy. *Mater. Res. Express* **2021**, *8*, 026518. [[CrossRef](#)]
9. Valiev, R.; Murashkin, M.Y.; Sabirov, I. A nanostructural design to produce high-strength Al alloys with enhanced electrical conductivity. *Scr. Mater.* **2014**, *76*, 13–16. [[CrossRef](#)]
10. Ye, H.; Cui, X.; Li, X.; Cui, H.; Zhang, B.; Li, H.; Pan, Y.; Feng, R.; Wu, Y.; Liu, X. Fabrication of hypoeutectic Al-4Si alloy with high electrical conductivity, high plasticity and medium strength by the dual treatment of Al matrix and eutectic Si microstructure. *J. Alloys Compd.* **2021**, *885*, 161117. [[CrossRef](#)]
11. Li, J.; Wang, X.; Ludwig, T.; Tsunekawa, Y.; Arnberg, L.; Jiang, J.; Schumacher, P. Modification of eutectic Si in Al–Si alloys with Eu addition. *Acta Mater.* **2015**, *84*, 153–163. [[CrossRef](#)]
12. Li, K.; Zhang, J.; Chen, X.; Yin, Y.; He, Y.; Zhou, Z.; Guan, R. Microstructure evolution of eutectic Si in Al-7Si binary alloy by heat treatment and its effect on enhancing thermal conductivity. *J. Mater. Res. Technol.* **2020**, *9*, 8780–8786. [[CrossRef](#)]
13. Han, S.Z.; Choi, E.-A.; Lim, S.H.; Kim, S.; Lee, J. Alloy design strategies to increase strength and its trade-offs together. *Prog. Mater. Sci.* **2021**, *117*, 100720. [[CrossRef](#)]
14. Wang, K.; Li, W.; Xu, W.; Hou, S.; Hu, S. Simultaneous Improvement of Thermal Conductivity and Strength for Commercial A356 Alloy Using Strontium Modification Process. *Met. Mater. Int.* **2020**, 1–15. [[CrossRef](#)]
15. Yang, C.-L.; Li, Y.-B.; Dang, B.; Lü, H.-B.; Liu, F. Effects of cooling rate on solution heat treatment of as-cast A356 alloy. *Trans. Nonferrous Met. Soc. China* **2015**, *25*, 3189–3196. [[CrossRef](#)]
16. Vandersluis, E.; Ravindran, C. Effects of solution heat treatment time on the as-quenched microstructure, hardness and electrical conductivity of B319 aluminum alloy. *J. Alloys Compd.* **2020**, *838*, 155577. [[CrossRef](#)]
17. VanderSluis, E.; Ravindran, C. Influence of solidification rate on the microstructure, mechanical properties, and thermal conductivity of cast A319 Al alloy. *J. Mater. Sci.* **2018**, *54*, 4325–4339. [[CrossRef](#)]
18. Mao, G.; Yan, H.; Zhu, C.; Wu, Z.; Gao, W. The varied mechanisms of yttrium (Y) modifying a hypoeutectic Al–Si alloy under conditions of different cooling rates. *J. Alloys Compd.* **2019**, *806*, 909–916. [[CrossRef](#)]
19. Li, L.; Li, D.; Mao, F.; Feng, J.; Zhang, Y.; Kang, Y. Effect of cooling rate on eutectic Si in Al-7.0Si-0.3Mg alloys modified by La additions. *J. Alloys Compd.* **2020**, *826*, 154206. [[CrossRef](#)]
20. Olafsson, P.; Sandström, R.; Karlsson, A. Comparison of experimental, calculated and observed values for electrical and thermal conductivity of aluminium alloys. *J. Mater. Sci.* **1997**, *32*, 4383–4390. [[CrossRef](#)]
21. Lumley, R.N.; Deeva, N.; Larsen, R.; Gembarovic, J.; Freeman, J. The Role of Alloy Composition and T7 Heat Treatment in Enhancing Thermal Conductivity of Aluminum High Pressure Diecastings. *Met. Mater. Trans. A* **2013**, *44*, 1074–1086. [[CrossRef](#)]
22. Cho, Y.H.; Kim, H.; Lee, J.M.; Kim, M.S. A new approach to the design of a low Si-added Al–Si casting alloy for optimising thermal conductivity and fluidity. *J. Mater. Sci.* **2015**, *50*, 7271–7281. [[CrossRef](#)]
23. Goulart, P.R.; Spinelli, J.; Osório, W.R.; Garcia, A. Mechanical properties as a function of microstructure and solidification thermal variables of Al–Si castings. *Mater. Sci. Eng. A* **2006**, *421*, 245–253. [[CrossRef](#)]
24. Bouchard, D.; Kirkaldy, J.S. Scaling of intragranular dendritic microstructure in ingot solidification. *Metall. Mater. Trans. B* **1996**, *27*, 101–113. [[CrossRef](#)]
25. Liao, H.; Sun, Y.; Sun, G. Correlation between mechanical properties and amount of dendritic α -Al phase in as-cast near-eutectic Al–11.6% Si alloys modified with strontium. *Mater. Sci. Eng. A* **2002**, *335*, 62–66. [[CrossRef](#)]

-
26. Liao, H.C.; Ding, Y.; Sun, G.X. Correlation between mechanical property and amount of dendritic α phase in near-eutectic Al-Si alloys modified with strontium. *Zhuzao Foundry* **2002**, *51*, 148. [[CrossRef](#)]
 27. Reddy, P.; Castelino, K.; Majumdar, A. Diffuse mismatch model of thermal boundary conductance using exact phonon dispersion. *Appl. Phys. Lett.* **2005**, *87*, 211908. [[CrossRef](#)]